Evaluation of Remote Sensing Aerial Systems In Existing Transportation Practices

1. Report No.	2. Government Accession No.	3. Recipient's Catalog No.
4. Title and Subtitle Evaluation of remote Sending Aerial Systems In Existing Transportation Practices		5. Report Date October 2009 6. Performing Organization Code
7. Author(s) Yu Gu		8. Performing Organization Report No. WVU-2008-01
9. Performing Organization Name and Address West Virginia University PO Box 6103 Morgantown, WV 26505		10. Work Unit No. (TRAIS) 11. Contract or Grant No. DTRT07-G-0003
12. Sponsoring Agency Name and Address U.S. Department of Transportation Research and Innovative Technology Administration UTC Program, RDT-30 1200 New Jersey Ave., SE Washington, DC 20590 West Virginia Department of Highway Donny Williams Building 5 1900 Kanawha Blvd E Charleston, WV 25305		13. Type of Report and Period Covered Final Report 07/01/2008-06/30/2009 14. Sponsoring Agency Code
15. Supplementary Notes		

16. Abstract

The application of small Remotely-Controlled (R/C) aircraft for aerial photography presents many unique advantages over manned aircraft due to their lower acquisition cost, lower maintenance issue, and superior flexibility. The extraction of reliable information from these images could benefit DOT engineers in a variety of research topics including, but not limited to work zone management, traffic congestion, safety, and environmental.

During this effort, one of the West Virginia University (WVU) R/C aircraft, named 'Foamy', has been instrumented for a proof-of-concept demonstration of aerial data acquisition. Specifically, the aircraft has been outfitted with a GPS receiver, a flight data recorder, a downlink telemetry hardware, a digital still camera, and a shutter-triggering device. During the flight a ground pilot uses one of the R/C channels to remotely trigger the camera. Several hundred high-resolution geo-tagged aerial photographs were collected during 10 flight experiments at two different flight fields.

A Matlab based geo-reference software was developed for measuring distances from an aerial image and estimating the geo-location of each ground asset of interest. A comprehensive study of potential Sources of Errors (SOE) has also been performed with the goal of identifying and addressing various factors that might affect the position estimation accuracy. The result of the SOE study concludes that a significant amount of position estimation error was introduced by either mismatching of different measurements or by the quality of the measurements themselves. The first issue is partially addressed through the design of a customized Time-Synchronization Board (TSB) based on a MOD 5213 embedded microprocessor. The TSB actively controls the timing of the image acquisition process, ensuring an accurate matching of the GPS measurement and the image acquisition time. The second issue is solved through the development of a novel GPS/INS (Inertial Navigation System) based on a 9-state Extended Kalman Filter (EKF). The developed sensor fusion algorithm provides a good estimation of aircraft attitude angle without the need for using expensive sensors. Through the help of INS integration, it also provides a very smooth position estimation that eliminates large jumps typically seen in the raw GPS measurements.

17. Key Words	18. Distribution Statement		
Remote Controlled Aircraft, Aerial Photography, Aerial data accusation	No restrictions. This document is available from the National Technical Information Service, Springfield, VA 22161		
19. Security Classif. (of this report) Unclassified	20. Security Classif. (of this page) Unclassified	21. No. of Pages	22. Price

Evaluation of Remote Sensing Aerial Systems In Existing Transportation Practices

Abstract

The application of small Remotely-Controlled (R/C) aircraft for aerial photography presents many unique advantages over manned aircraft due to their lower acquisition cost, lower maintenance issue, and superior flexibility. The extraction of reliable information from these images could benefit DOT engineers in a variety of research topics including, but not limited to work zone management, traffic congestion, safety, and environmental.

During this effort, one of the West Virginia University (WVU) R/C aircraft, named 'Foamy', has been instrumented for a proof-of-concept demonstration of aerial data acquisition. Specifically, the aircraft has been outfitted with a GPS receiver, a flight data recorder, a downlink telemetry hardware, a digital still camera, and a shutter-triggering device. During the flight a ground pilot uses one of the R/C channels to remotely trigger the camera. Several hundred high-resolution geo-tagged aerial photographs were collected during 10 flight experiments at two different flight fields.

A Matlab based geo-reference software was developed for measuring distances from an aerial image and estimating the geo-location of each ground asset of interest. A comprehensive study of potential Sources of Errors (SOE) has also been performed with the goal of identifying and addressing various factors that might affect the position estimation accuracy. The result of the SOE study concludes that a significant amount of position estimation error was introduced by either mismatching of different measurements or by the quality of the measurements themselves. The first issue is partially addressed through the design of a customized Time-Synchronization Board (TSB) based on a MOD 5213 embedded microprocessor. The TSB actively controls the timing of the image acquisition process, ensuring an accurate matching of the GPS measurement and the image acquisition time. The second issue is solved through the development of a novel GPS/INS (Inertial Navigation System) based on a 9-state Extended Kalman Filter (EKF). The developed sensor fusion algorithm provides a good estimation of aircraft attitude angle without the need for using expensive sensors. Through the help of INS integration, it also provides a very smooth position estimation that eliminates large jumps typically seen in the raw GPS measurements.

Table of Contents

List of Figures

List of Tables

Evaluation of Remote Sensing Aerial Systems In Existing Transportation Practices

1. Introduction

1.1. Background

Aerial photography has long been used for tactical assessment and planning purposes, relying primarily on manned aircraft. It has also found various applications in transportation infrastructure planning and monitoring in the civilian sector. However, the higher cost and risks to humans associated with the use of manned aircraft for such purposes has made it prohibitive for extensive applications. The associated logistic burden and preparation time for a full-scale aircraft also limited its use during emergency situations.

The rapid evolution of the small Remotely Piloted Vehicle (RPV) and Unmanned Aerial Vehicle (UAV), coupled with the miniaturization of sensors, computers, and communication equipments, has led to an increased use of this class of platforms in the civilian sector, especially within the framework of Intelligent Transportation Systems (ITS). Typical data that are collected with an airborne platform are aerial photographs of roads and other transportation infrastructure. For example, researchers from Bridgewater State College used regular off the shelf film cameras to capture images of parking lots associated with park and ride shuttles. The camera was mounted on a small hand launched Micro Aerial Vehicle (MAV) controlled by a ground-based pilot with the aid of a video downlink from the vehicle [1]. In another application, UAVs were used to provide a cost effective "system solution" for use in aerial surveillance, right of way monitoring and leak detection of pipelines [2]. The use of UAVs in law enforcement related to traffic management has been gaining traction, especially in foreign countries. In Israel, real time

video footage of traffic violations are captured from small unmanned helicopters and transmitted to patrol cars to apprehend traffic violators [3]. The video footage from the UAV is considered to be admissible evidence in a court of law and is used to support the testimony of law enforcement personnel trained in traffic patrolling from the air. Another application is the use of UAVs in support of the first responders. MIRAMAP and E-Producties in Europe have designed a helicopter system that can be rapidly deployable and is able to collect real-time color and thermal infrared video images that are sent to a command and control center. It is also capable of collecting high-resolution geo-referenced digital imagery that is made available to first responders on existing GIS platforms in open GIS formats in a short time after a disaster [4].

Unmanned helicopters have been used in the United States for Photogrammetric mapping and monitoring of the conditions of unpaved roads, sponsored by the US DOT [5]. This study was aiming for timely identification and rectification of road deformation through loss of crown or damage to the road base. The automatically controlled helicopter can fly along predefined flight paths; and is equipped with a Global Positioning System (GPS)/Inertial Measurement Unit (IMU) and a geomagnetic sensor to detect the position, attitude and velocity of the platform.

The University of South Florida (USF) has been actively involved in cooperative research projects with the Florida Department of Transportation to investigate and design an Airborne Traffic Surveillance System (ATSS). ATSS is based on an Aerosonde UAV platform, and features digital video encoding, and transmission of data and multimedia video streams over FDOT's microwave IP networks. This is designed to be an improvement over the current DOT practices such as fixed tower mounted cameras or embedded detectors, and provides a "bird's

eye view" to obtain data on traffic trends as well as to monitor and control traffic, monitor road conditions, and coordinate emergency response [6,7,8].

In addition to typical UAV deployment scenarios for remote traffic monitoring and offline analysis of traffic patterns [9-12], several recent efforts have also attempted to add reasoning capabilities to UAVs used for traffic surveillance. In one such application, with the central idea of traffic surveillance over a widely varying geographical terrain (covering networks in city, suburban and rural areas, both densely and sparsely populated), the UAV is equipped to "understand" the situation on the ground [13]. Such a capability aimed to interpret patterns such as conventional maneuvers of a vehicle, dangerous or otherwise exceptional maneuvers, and structure of the traffic such as congestion. The UAV is also capable of performing tasks that are assigned by the ground operator or automatically triggered by the observations it interprets. For example, to follow a vehicle that flees from the scene of an apparent crime, or to assist a vehicle through difficult traffic conditions or to re-route traffic and get to a particular destination as quickly as possible. In another such application, a system was implemented to achieve high-level situation awareness about traffic situations in an urban area [14]. This uses sequences of color and thermal images from the UAV as inputs to construct and maintain qualitative object structures and to recognize the traffic behavior in real time. Along the same lines, UAVs with capabilities to conduct autonomous search and track missions have been used in surveillance operations include inspecting and monitoring river boundaries, bridges and coastlines [15]. In this project, a fixed wing UAV equipped with on-board vision or infrared sensors is applied to search and map littoral boundaries based on visual feedback.

Although there have been several successful demonstrations of small RPVs and UAVs in monitoring and managing traffic flow, detecting pipeline leaks, and collecting imagery for environmental, safety, security, and emergency management applications there still exist a number of barriers to a wide scale UAV deployment. This could hamper any planned demonstrations in the future and prevent rapid technology transfer into transportation practice. Currently, there is an effort to identify barriers to near-term UAV deployment for diverse transportation safety and security applications and the eventual development of a simple set of guidelines, or Standard Operating Practices (SOP) for UAV deployment by states and local transportation agencies, or by other transportation system owners or operators [16].

1.2. Regulations

While the use of small UAVs in traffic monitoring has become increasingly popular, the widespread deployment of such systems in the civilian airspace is still restricted by the Federal Aviation Administration (FAA) regulations. FAA have so far issued two Interim Operational Approval Guidance (AFS-400 UAS Policy 05-01 [17], dated September 16, 2005, and 08-01 [18], dated March 13, 2008) regulating the Unmanned Aircraft Systems (UAS) operations in the U. S. National Airspace System (NAS).

Particularly, Interim Operational Approval Guidance 08-01 states that: "*In general, specific authorization to conduct unmanned aircraft operations in the NAS outside of active Restricted, Prohibited, or Warning Area airspace must be requested by the applicant. Airspace inside buildings or structures is not considered to be part of the NAS and is not regulated. The two methods of approval are either a certificate of waiver or authorization (COA) or the issuance of a special airworthiness certificate.*"

"*The applicability and process to be used in a UAS operational approval is dependent on whether the applicant is a civil user or a public user. A public user is one that is intrinsically governmental in nature (i.e., federal, state, and local agencies). Public applicants should utilize the COA application process. Civil applicants must apply for an airworthiness certificate.*"

In general, the FAA's primary concern is that Unmanned Aircraft (UA) operates safely among non-cooperative aircraft and other airborne operations not reliably identifiable by RADAR, i.e. balloons, gliders, etc.

For the use of Remote Control (R/C) model aircraft, FAA does not provide specific regulations. Advisory Circular (AR 91-57) [19], dated June 9, 1981 refers to the subject of 'model aircraft operating standards', specifically outlining the compliance with safety standards for model aircraft operators. The operating standards describe include:

a. *"Select an operating site that is of sufficient distance from populated areas. The selected site should be away from noise sensitive areas such as parks, schools, hospitals, churches, etc;"*

b. *"Do not operate model aircraft in the presence of spectators until the aircraft is successfully flight tested and proven airworthy;"*

c. *"Do not fly model aircraft higher than 400 feet above the surface. When flying aircraft within 3 miles of an airport, notify the airport operator, or when an air traffic facility is located at the airport, notify the control tower, or flight service station;"*

d. *"Give right of way to, and avoid flying in the proximity of, full-scale aircraft. Use observers to help if possible;"*

e. *"Do not hesitate to ask for assistance from any airport traffic control tower or flight service station concerning compliance with these standards."*

The operation of R/C model aircraft should also follow the rules of the AMA (Academy of Model Aeronautics), which requires keeping the weight of the UAV under 55 lbs. and flying within visual range of the ground pilot under a 400 ft altitude ceiling [20].

According to FAA Notice of Policy FAA-2006-25714 [21]: "*The FAA has undertaken a safety review that will examine the feasibility of creating a different category of unmanned "vehicles" that may be defined by the operator's visual line of sight and are also small and slow enough to adequately mitigate hazards to other aircraft and persons on the ground. The end product of this analysis may be a new flight authorization instrument similar to AC 91-57, but focused on operations which do not qualify as sport and recreation, but also may not require a certificate of airworthiness. They will, however, require compliance with applicable FAA regulations and guidance developed for this category.*"

1.3. Objective of the Project

The main objective of this project is to evaluate the possibility of implementing flexible, intelligent, and low-cost remotely controlled data acquisition solutions complementing existing DOT measurement systems by supplying high-quality aerial imagery for various aspects of the highway research and operations.

1.4. Organization of the Report

This report is divided into five chapters. Chapter 1 describes the background of the research, the FAA and AMA regulations, and the objectives of the project. Chapter 2 discusses the development of the aerial platform, specifications for key components, and results of the flight-testing operations. Chapter 3 discusses the development of the geo-referencing software, followed by a detailed analysis of various Sources of Errors (SOE) and the associated corrective procedures. Chapter 4 outlines a sensor fusion algorithm able of estimating the aircraft attitude angle as well as improving positioning accuracy based on information from both GPS and a low-cost INS (Inertial Navigation System). Chapter 5 provides the conclusions and outlines the follow-up research activities.

2. Aerial Platform Development and Flight Testing

Within this effort, one of the West Virginia University (WVU) remotely piloted aircraft, named 'Foamy', has been customized for data acquisition purpose. The 'Foamy' aircraft was selected because of its low cost and flexibility in accommodating different sensor payloads. A brief description of the 'Foamy' platform is provided in Table 1.

Length	70.1" (1.8 m)
Wingspan	67" (1.7 m)
Wing Cord	Root 19.7" (0.5 m), Tip 7.87" (0.2 m)
Weight (Aircraft only)	9.92 lb (4.5 Kg)
Maximum Takeoff Weight	13.50 lb (6.1 Kg)
Engine	GMS 0.76, 2-stroke glow engine, 2.5 hp
Typical Flight Duration	10 Minutes

Table 1. General Specifications of the WVU 'Foamy' Aircraft

The overall layout of the instrumented 'Foamy' aircraft is shown in Figures 1-2. The current avionic components include a Remote Control (R/C) system, a GPS receiver, a flight data recorder, downlink telemetry hardware, a digital still camera, and a shutter-triggering device. During the flight the ground pilot use one of the R/C channels to remotely trigger the camera.

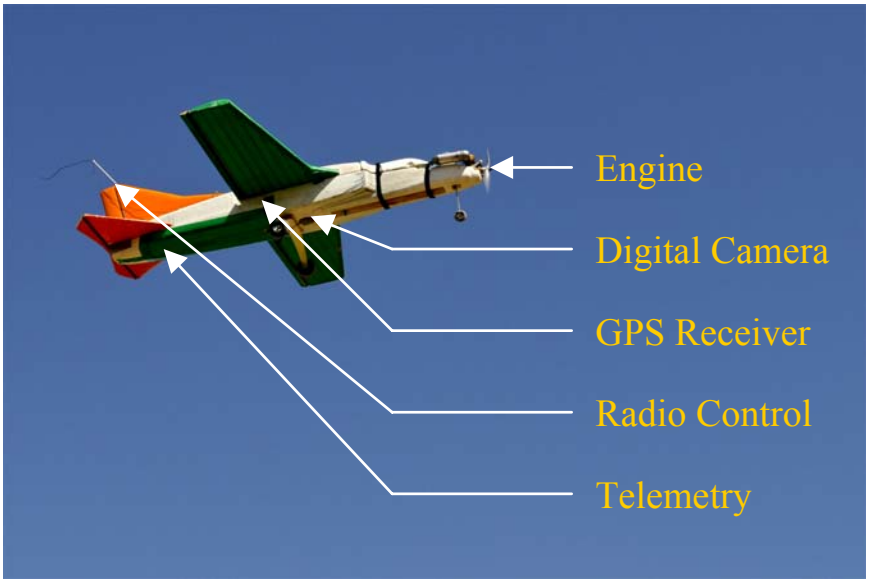

Fig. 1. Foamy Aircraft Configuration

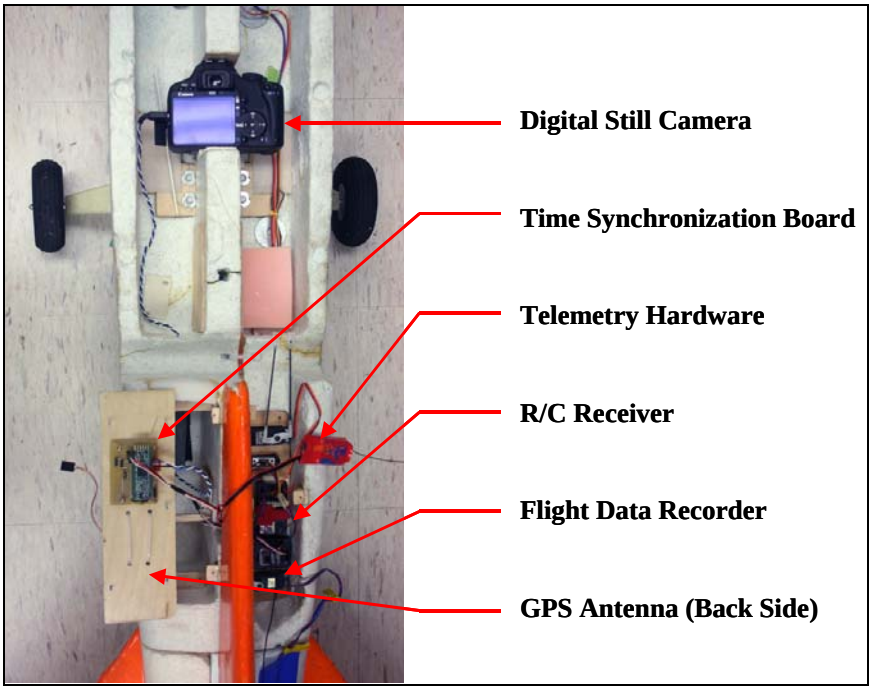

Fig. 2. A Close Up of the Aircraft Internal Configuration

Two digital cameras are used for this project. The first camera is 'off-the-shelf' Canon Digital Rebel XTi mainly used for visible spectrum photography. Another camera is a Canon Digital Rebel T1i. This camera was professionally modified to have the internal Infrared-block filter removed and replaced with an external Infrared-pass filter. This camera is mainly used for near-Infrared photography. Both cameras have similar footprints so they are interchangeable inside the aircraft and they share the same shutter triggering mechanism. Two camera lenses were tested during initial flights: a 50mm F1.8 fixed focal length lens and an 18-55mm F3.5-5.6 zoom lens. The 18-55mm lens when locked at 18mm was eventually proven to be more suitable for this particular application and was used in most subsequent flight tests. Key specifications for both cameras that are directly related to aerial photography are shown in Table 2.

	Canon Digital Rebel XTi	**Canon Digital Rebel T1i**
Max resolution	3888 x 2592	4752 x 3168
Effective pixels	10.1 million	15.1 million
Sensor size	22.2 x 14.8 mm (3.28 cm²)	22.3 x 14.9 mm (3.32 cm²)
ISO rating	100-1600	Auto, 100-3200
Max shutter	1/4000 sec	1/4000 sec
Focal length multiplier	1.6	1.6
Continuous Drive	3.0 fps, 27 JPEG	3.4 fps, 170 JPEG
Movie Clips	N/A	1920 x 1080 @ 20 fps, 1280 x 720 @ 30 fps
Remote control	E3 connector, InfraRed	E3 connector, InfraRed
Battery	720mAh Li-Ion	1050mAh Li-Ion
Weight (inc. batteries)	19.6 oz (556 g)	18.3 oz (520 g)
Dimensions	5" x 3.7" x 2.6" (127 x 94 x 65 mm)	5.1" x 3.9" x 2.4" (129 x 98 x 62 mm)

Table 2. Camera Specifications

The flight data recorder is based on an Eagletree® Seagull Wireless Dashboard Telemetry and Data Recorder System. It provides basic functions of logging GPS data, record pilot command, and sending data to the ground station. General Specifications for the Eagletree system are listed in Table 3.

Data Recorder	
Operational Voltage	4.35V to 7.0V
Weight	1 oz (28 g)
Dimensions	1.97” x 1.38” x 0.67” (50 x 35 x 17 mm)
Record Time	Approx. 20 minutes
FCC 900 MHz, 200mW Transmitter	
Power:	Power Taken from Recorder/Receiver Battery
Current Draw	Transmitter + Recorder, average < 70 milliamp
Frequency Range	902 – 928 MHz
Operating Range (Line of Sight)	Up to 1.2 miles w/included antenna
Weight	Approx 0.5 oz (14g, Transmitter only)
Dimensions	2.75” x 1.25” x 0.25” (70 x 32 x 6 mm)
GPS Expander	
Update Rate	5Hz
WAAS and EGNOS Support	Yes
Time to Fix	Less Than 1 Second Hot, 36 Second Cold (Typical)
Speed Accuracy	Approx 0.1 m/s
Current draw	Less Than 40 mA Steady State
Weighs	Approx 0.4 oz (11g)
Dimensions	1.4” x 0.6” x 0.3” (35x16x8mm)
Position accuracy	Approx 8.2 ft (2.5m) CEP

Table 3. Eagle Tree Specifications

Two flight sessions with a total of six flights have been conducted at the WVU Jackson’s Mill flight-testing facility. An additional flight session with eight flights was performed at Friendship Hill, Point Marion, PA. A GPS trajectory overlaying a 3D Google Earth map is presented in Figure 3, shown the aircraft circling over Friendship Hill.

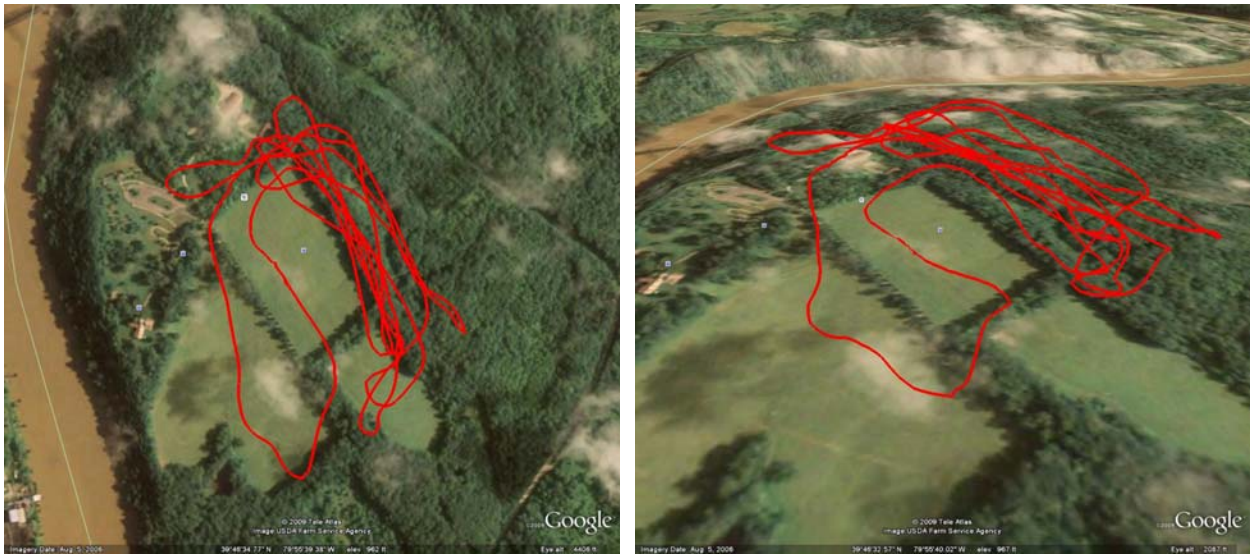

Fig. 3. Flight Trajectory Over the Friendship Hill

Several hundred high-resolution geo-tagged aerial photographs were taken during these flight experiments. A single frame of an aerial photograph collected at Jackson's Mill is presented in Figure 4; the image provides a high-resolution coverage of a construction site.

Fig. 4. A Single Aerial Photo

A mosaic of 16 aerial images collected from a different flight test is also shown in Figure 5.

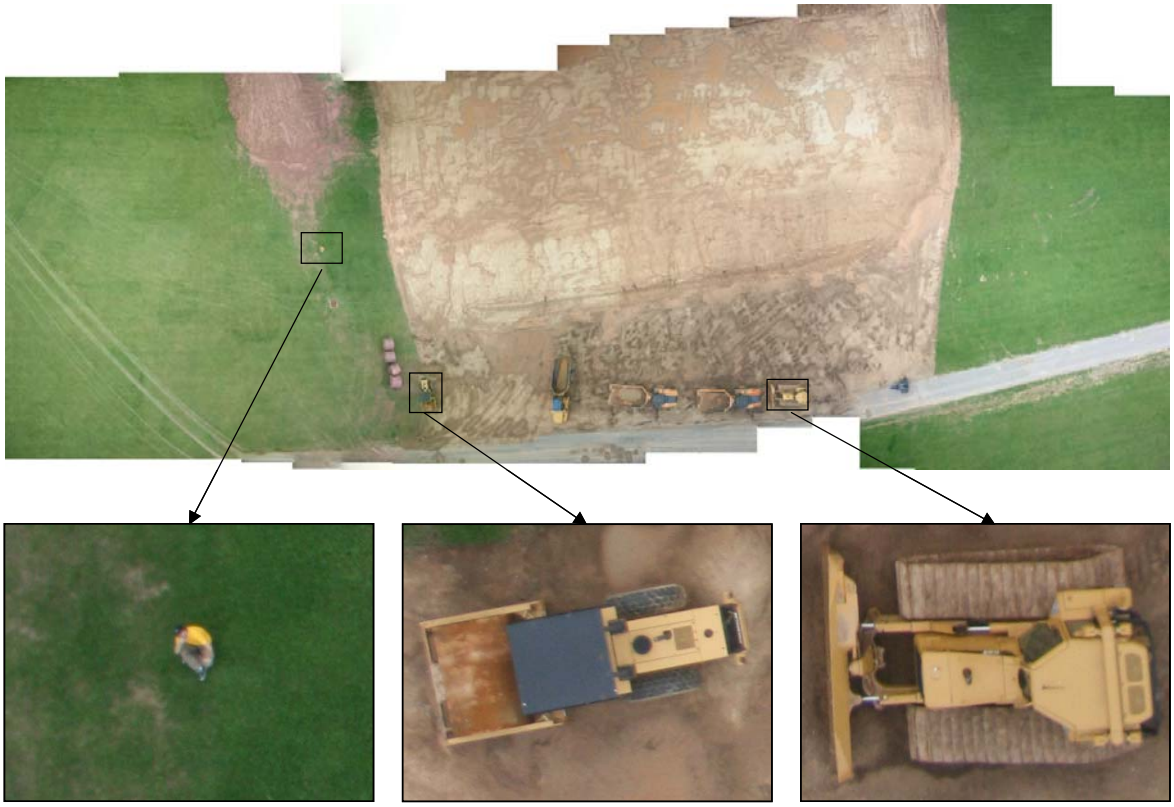

Fig. 5. A Mosaic of 16 Aerial Images

3. Data Processing and Error Analysis

3.1 Geo-Referencing Software

To utilize the collected aerial photos for DOT applications, a geo-referencing software was developed within this effort. By definition, geo-referencing a photo implies the derivation of a correct mapping between the center of the photo and its geographical coordinates, commonly in terms of Latitude and Longitude. Following a successful geo-reference for one point, it is then theoretically possible to geo-reference any other point in the image through simple geometric

calculations. Although conceptually straightforward, the measurement of a distance on an aerial image, along with the consequent positioning of objects in the picture, presents several technical challenges and it is sensitive to several Sources of Errors (SOE).

A Matlab® script was developed for computing distances and latitude/longitude for points selected by the user on a picture, from a central point of known coordinates. The script requires some parameters to be set up by the user, which are:

***hs, vs*:** height and width of sensor or film of the camera used. These parameters are needed for computation of Field of View (FOV) and Angle of View (AOV) from a certain height above the ground;

***f*:** focal length of the lens used when taking the picture;

***H*:** height above the ground when the picture was taken.

The determination of ratios between the physical dimension and the pixel count depend on the proper setting of above parameters. Additionally, the transformation of longitude and latitude measurements in degrees to distance in meters is based on equations supplied by the National Geospatial – Intelligence Website [22]. If ϕ is the current latitude, then the length of a degree of latitude ϕ^{1° can be calculated by:

$$M(\phi) = \frac{(ab)^2}{\left((a\cos(\phi))^2 + (b\sin(\phi))^2\right)^{3/2}} \tag{1}$$

$$\phi^{1^\circ} = \frac{\pi}{180} M(\phi) \tag{2}$$

where ϕ^{1° is in meters; a and b are, respectively, the equatorial and polar radii of Earth, they can be approximated to be *6378137m* and *6356752m* based on the datum used for earth shape modeling. These radii are the ones used on the WGS84 datum ellipsoid, which is the most common for GPS applications.

The length of a degree of longitude τ^{1° is obtained by the formula:

$$\tau^{1^\circ} = \frac{\pi}{180^\circ}\cos(\phi)\sqrt{\frac{a^4\cos(\phi)^2 + b^4\sin(\phi)^2}{(a\cos(\phi))^2 + (b\sin(\phi))^2}} \tag{3}$$

Then longitude and latitude of the central position are loaded from the GPS measurement, in the following format: ***lon/lat*** = [deg min.decimal]. The heading of the aircraft, ***hdg*** in radians, is also estimated from GPS readings. The FOV from a certain distance are estimated to be:

$$h_{FOV} = H\frac{h_s}{f} \tag{4}$$

$$v_{FOV} = H\frac{v_s}{f} \tag{5}$$

with h_{FOV} being the horizontal FOV in meters, and v_{FOV} is the vertical FOV.

The calculation of the AOV is performed using:

$$h_{AOV} = 2\arctan\left(\frac{h_s}{2f}\right) \tag{6}$$

$$v_{AOV} = 2\arctan\left(\frac{v_s}{2f}\right) \tag{7}$$

After loading the photo into Matlab, a conversion factor between pixels and "real" length can be computed as:

$$p2m = \frac{h_{FOV}}{h_{IMAGE}} \tag{8}$$

with h_{IMAGE} being the horizontal number of pixels of the image. Since square pixels were used in our cameras, vertical and horizontal factors are the same, even if this is not true for the length as acquired from the lens. This means that a source of error is the fact that the lens at low focal distances (*f*) tends to transform squares into rectangles; therefore, the 90° angles are not exactly preserved. The distances from the central position are calculated as:

$$h_{DIST} = x_P - \frac{h_{IMAGE}}{2} \tag{9}$$

$$v_{DIST} = y_P - \frac{v_{IMAGE}}{2} \tag{10}$$

where x_P and y_P are the pixel coordinates of the points, as selected by the user with a simple point-and-click GUI shown in Figure 6.

Fig. 6. GUI for Point-and-Click Acquisition of Points, Black Arrow is the North-Direction

The number of points to be clicked and acquired can be selected by the user. The length of the distance vector from the center is computed as:

$$t_{DIST} = \sqrt{h_{DIST}^2 + v_{DIST}^2} \tag{11}$$

All the pixel distances can then be converted to real distances, with factors described earlier. The next step is to compute the rotation between the heading and the vector to point, so that we can pass from the local reference system to a global reference system (North-East). If the direction angle of the distance vector is:

$$\xi = \arctan\left(\frac{h_{DIST}}{-v_{DIST}}\right) \tag{12}$$

Then the angle between true North and this vector, which will be the angle needed for projecting the distances from local to global system, is:

$$\omega = hdg - \xi \tag{13}$$

Consequently, the distances in the global reference are:

$$N_{DIST} = t_{DIST} \cdot \cos(\omega) \tag{14}$$

$$E_{DIST} = -t_{DIST} \cdot \sin(\omega) \tag{15}$$

Finally, the correction in terms of degree for longitude and latitude can be computed with the length inserted above, as:

$$\Delta_{LON} = \frac{E_{DIST}}{\tau^{1^\circ}} \tag{16}$$

$$\Delta_{LAT} = \frac{N_{DIST}}{\phi^{1^\circ}} \tag{17}$$

Therefore, the longitude and latitude of the points will be:

$$LON_P = lon + \Delta_{LON} \tag{18}$$

$$LAT_P = lat + \Delta_{LAT} \tag{19}$$

The software can be used either to offset the coordinate of a point from the center or as a tool for measuring the distances; the concepts are the same, and only a conversion from metric distances to degree of angle is involved.

As an example of the use of this software, we tried to estimate the wingspan of a Cessna 172. The picture shown in Figure 7 was taken from a height of approximately 51 m (171 ft) with a Canon Rebel XTi, mounting a standard 18-55 mm zoom lens locked at 18mm.

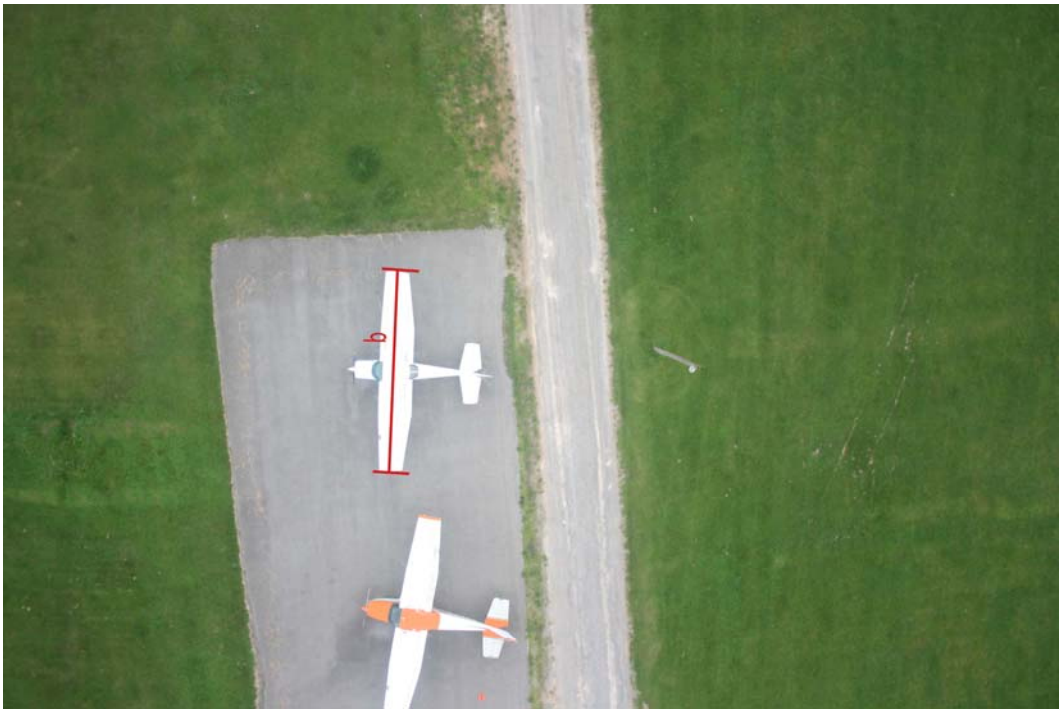

Fig. 7. Aerial Photo of Two Cessna Aircraft

With two clicks on each wingtip the program performs the calculations and the result is b=12.187m. Known that the actual wingspan of a Cessna 172 is 11m the associated estimation error is approximately 10%, compatible with the error expected on the measurement of the height of the aircraft due to the time synchronization. The output of the script is in Figure 8,

Horizontal field of view with 18 mm lens from 52.1208 meters:
64.2823
Vertical field of view with 18 mm lens from 52.1208 meters:
42.8549
dist_21 =
12.1870
lon_point =
-80.0000 28.2006
-80.0000 28.1990
lat_point =
39.0000 5.6578
39.0000 5.6643

Fig. 8. Output of the Script

where *lat_point* and *lon_point* are the coordinates of the selected points.

The initial evaluation of the script shows a typical position estimation error of 40-50 meters when compared with the ground 'true' measurement using a handheld GPS unit. If a landmark with known position is shown in the same image, the position estimation error can be substantially reduced. Efforts have then focused on the identification of potential sources of errors and design corrective measures accordingly.

3.2. Source of Error

The possible Sources of Error (SOE) in the measurement of distances from aerial photos can be roughly divided into two classes: "Before Acquisition -BA" and "After Acquisition - AA". The BA class includes all those errors that do not depend on the picture itself, such as GPS error, positioning error, and other hardware errors. Errors from the AA class are related to the

fact that distances are measured from a picture; therefore, AA errors include lens distortions, imprecision, and general problems in relating a pixel distance to a real distance. In the following sections each identified SOE is discussed, along with an estimate of its magnitude, whenever possible.

Matching Image with GPS positioning

This is the error associated with the matching of an image with corresponding GPS measurement. Since the on-board GPS provides the initial position of the central point of the picture, it is very important to achieve an accurate synchronization of the camera shutter with a recorded GPS position. If this is not done properly, the final position estimation error can be quite large. Assuming a synchronization error of 1 sec. between the time of the acquisition and the recorded position, we introduce an error that depends on the ground speed of the aircraft. Typical airspeed for the 'foamy' aircraft is around 20m/s, leading to a position estimation error of approximately 20m at the center of the image. To reduce this error, a time-synchronization board has been designed and developed for an accurate control of the time matching process. A detailed discussion of the time-synchronization board is provided in Section 3.3.

Attitude of the Aircraft

When the image is taken, the aircraft is likely not flying in a straight and level condition. This is a known problem for geo-referencing from an aerial photograph. As an estimate, if the aircraft flies at 52m above the ground, an angle δ [deg] will cause an error $e = H\tan(\delta)$ on the position estimation of the center of the picture. The relationship between angle and error is shown in Figure 9.

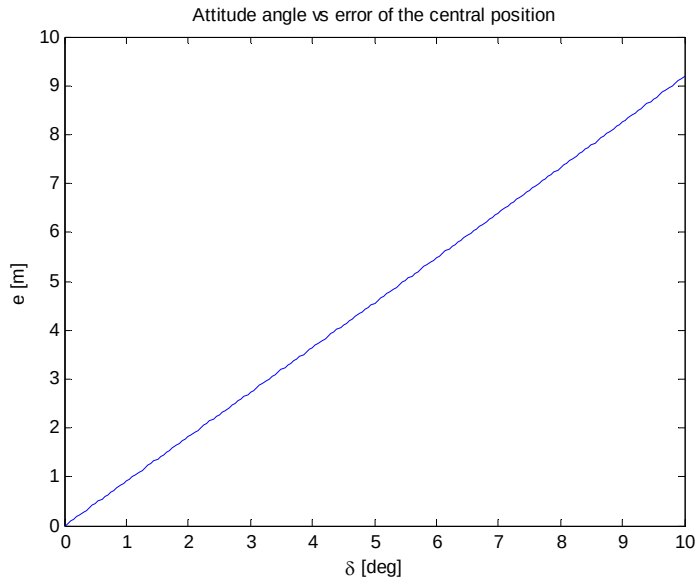

Fig. 9. Angle Errors vs. Position Error

Figure 9 shows that, for small angles, the relationship is close to be linear. From a height of 52m, an error of 5° leads to an error of approximately 5 meters. If an error of 5° is assumed on both pitch and roll, then a total error would be around 7 m on the diagonal positioning.

A possible solution for reducing these errors would be to mount the camera on an inertial (gimbaled) platform with the goal of maintaining the orientation of the camera for a range of aircraft attitude angles. This approach would effectively reduce the aforementioned errors, but with a penalty on weight, cost, and complexity. A more elegant and low-cost solution is to introduce a set of inertial sensors and sensor fusion techniques providing attitude angle estimates for post flight image transformation. Details about the sensor fusion algorithm development are provided in Section 4.

GPS Error

Any error during the GPS measurement will directly transfer itself to the final position estimation error. The GPS manufacture's specifications list a GPS measurement accuracy of 2.5m CEP (Circular Error Probability). However, this is believed to be a highly optimistic estimation, especially during dynamic flight conditions.

Summing the aforementioned SOEs, a total error of approximately **30m** on the final estimated position can be categorized as BA-Error.

Lens Distortion

This is a very common error and it originates from the distortion of most commercial lenses, especially wide-angle lenses. The type and severity of the distortion is strictly related to the specific lens used. There are two approaches for reducing this error: the first approach is based on the use of a longer focal length lens (e.g. 24mm instead of the 18mm setting used); however, this will have the drawback of restricting the field of view. A second approach is based on the use of specialized post-editing software. Since generating "orthophotos" from aerial images is a very wide field of study, there are many specialized codes for mapping "ortophotos". In particular, several commercial software packages feature a database of the correction parameters for many common commercial lenses.

The use of the commercially available software "PTLens" allows us to correct lens distortions in this study. The difference between the position of an object before and after the correction is presented in Figure 10, which superimposed the results with false color.

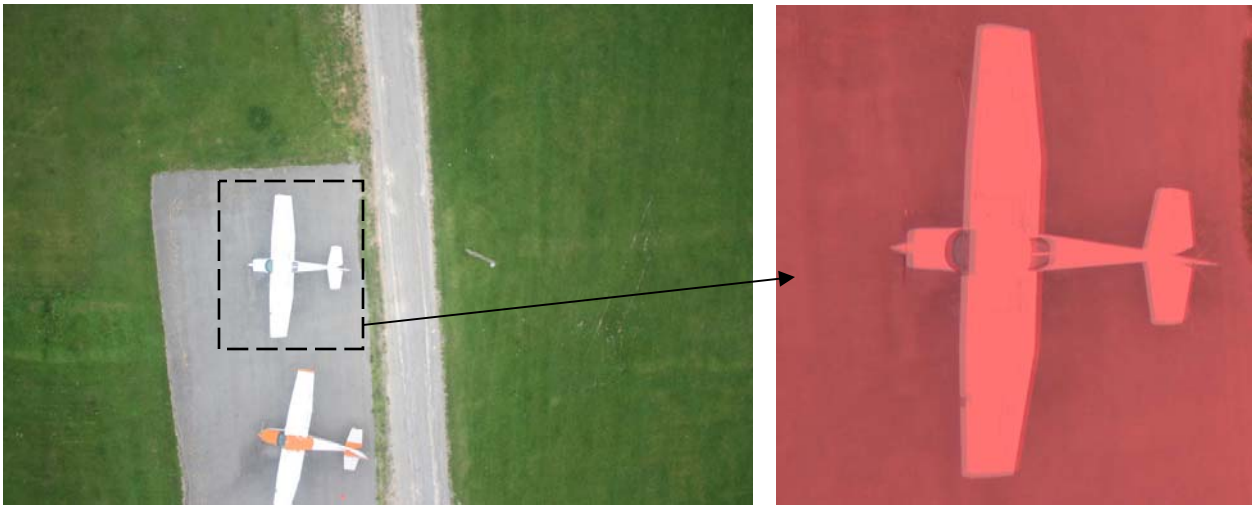

Fig. 10. Superimposition of Object Before and After Distortion Correction

Altitude Error

The altitude error is not a direct error by itself, as in theory the position of the center is not affected by the altitude of the aircraft. However, it becomes a source of error when the position of an object not on the centerline is measured. The relation between apparent dimensions and real dimension is strongly dependent on the distance. Again, there is a linear relationship between the error in altitude and the final estimation error.

3.3. Time-Synchronization Board

To reduce the error introduced by time gaps between the GPS measurements and the measured acquisition time of the images, a Time-Synchronization Board (TSB) has been developed for active control of the image acquisition process. The main idea is to develop a circuit board with an embedded microchip controlling the shutter of a camera, while sending PWM (Pulse Width Modulation) signals to the flight data-recorder. Since GPS Data-Recording hardware can record PWM signals, as they are used to control and register the position of electric actuators, a system like this allows the recording of a progressive number coming from the TSB

as an index of the picture taken at a certain time. This number is then associated with the GPS measurement to provide an accurate geo-tagging of each acquired image.

The TSB board is built around a NetBurner MOD-5213 embedded microprocessor, which is an integrated microchip used for control and communication applications. This device shows a great flexibility in generating PWM signals of the desired duty cycle to encode the image index. Associated with a variation in the PWM output of the MOD5213, the board can also send a voltage command to the camera, either turning on the autofocus or activating the shutter. The interval between pictures can be set up in the embedded software, written in C language. Anytime a picture is taken, the associated PWM reading channel on the flight data recorder will read an increased value from the PWM signal. Since all of these channels are logged, it is then possible to match pictures and GPS locations with desirable accuracy. The design for the circuitry of the TSB is presented in Figure 11.

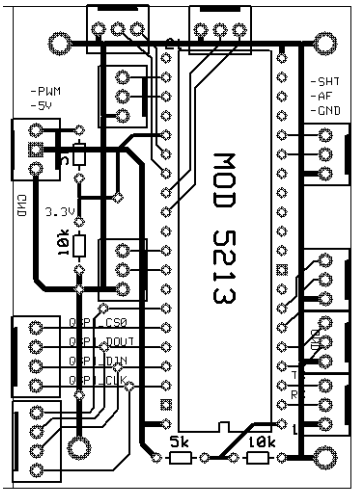

Fig. 11. Time-Synchronization Board (Circuitry)

The physical realization of this board is presented in Figure 12, where it is connected to a Canon Digital Rebel T1i camera.

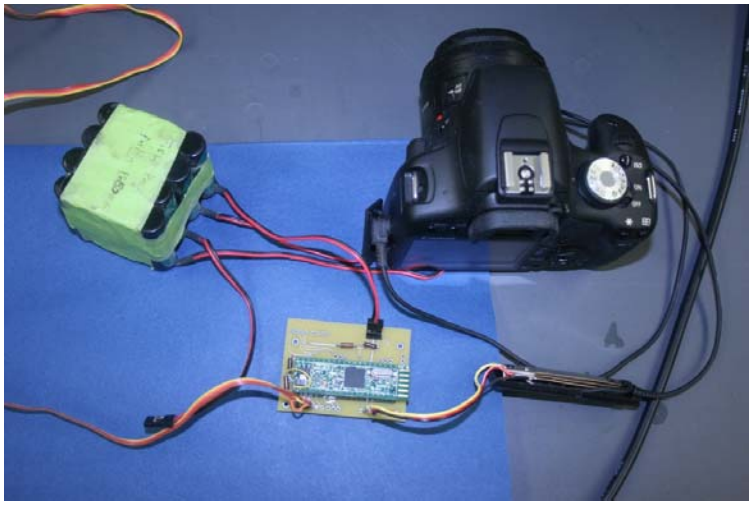

Fig. 12. Board Connected to the Camera

4. GPS/INS Sensor Fusion

The SOE analysis from the previous chapter shows that a significant amount of position estimation errors was introduced by either mismatching different measurements, or by the (low) quality of the measurements. The first issue is partially addressed through the design of a Time-Synchronization Board; the second issue can be solved using new sensors and novel methods for integrating their measurements. The integration of information from multiple-sources is a key approach toward improving the measurement reliability and to reduce the overall size, weight, and power consumption of an airborne system.

Within this research, two sets of information are required to further improve the position estimation performance: 1) aircraft attitude angles, and 2) accurate aircraft position information. The GPS receiver on-board the aircraft can only provide a coarse (in term of both spatial and

temporal resolution) measurement of the aircraft position. An alternative method used by most large aircraft and spacecraft is through the use of Inertial Navigation System (INS), which provides both attitude angle and position estimation. However, a navigation-grade INS is well beyond the price and weight range of our test-bed aircraft. Low cost Inertial Measurement Units (IMU) based on Micro-Electro-Mechanical Systems (MEMS) technology are commercially available at a reasonable price. However, low cost IMU has limited performance (drifting characteristics) and cannot be used for direct navigation purposes.

By properly integrating GPS and inertial sensor measurements, the unbiased nature of the GPS signals can limit the size of the low frequency errors in the inertial system. Similarly, the continuity of the INS can be used to fill in position information gaps between GPS updates and reduce the effect of high frequency GPS errors [23,24]. Therefore, the GPS/INS sensor fusion allows for substantial improvement of the performance and reliability of the position measurement system. Additionally, the velocity measurement from the GPS receiver can be used to estimate the aircraft acceleration vector. This vector is different from the acceleration vector measured by the accelerometers inside the IMU, which also include the acceleration due to Earth's gravity. By comparing the two sources of acceleration measurements, it is possible to compute the earth's gravitational vector with respect to the aircraft's body frame, leading to an estimation of aircraft attitude angles.

In this study, an Extended Kalman Filter based sensor fusion algorithm was developed to provide attitude angle estimation as well as more refined position estimation with a higher update rate. As described earlier, there are two types of sensors that could provide the acceleration information. One is the IMU, which directly measures the linear acceleration in the aircraft body

frame. Another source of information is provided by the GPS receiver, which measures 3-axis position and velocity in the Earth-Centered-Earth-Fixed (ECEF) frame. The accelerations along the ECEF frame can then be calculated by differentiating the GPS velocity solutions. The relationship between the two types of acceleration measurements is dependent on the aircraft Euler angles:

$$\begin{aligned}
\begin{bmatrix} \dot{V}_x \\ \dot{V}_y \\ \dot{V}_z + g \end{bmatrix} &= \begin{bmatrix} \cos\psi & -\sin\psi & 0 \\ \sin\psi & \cos\psi & 0 \\ 0 & 0 & 1 \end{bmatrix} \begin{bmatrix} \cos\theta & 0 & \sin\theta \\ 0 & 1 & 0 \\ -\sin\theta & 0 & \cos\theta \end{bmatrix} \begin{bmatrix} 1 & 0 & 0 \\ 0 & \cos\phi & -\sin\phi \\ 0 & \sin\phi & \cos\phi \end{bmatrix} \begin{bmatrix} a_x \\ a_y \\ a_z \end{bmatrix} \\
&= \begin{bmatrix} \cos\psi\cos\theta & -\sin\psi & \cos\psi\sin\theta \\ \sin\psi\cos\theta & \cos\psi & \sin\psi\sin\theta \\ -\sin\theta & 0 & \cos\theta \end{bmatrix} \begin{bmatrix} 1 & 0 & 0 \\ 0 & \cos\phi & -\sin\phi \\ 0 & \sin\phi & \cos\phi \end{bmatrix} \begin{bmatrix} a_x \\ a_y \\ a_z \end{bmatrix} \\
&= \begin{bmatrix} \cos\psi\cos\theta & -\sin\psi\cos\phi + \cos\psi\sin\theta\sin\phi & \sin\psi\sin\phi + \cos\psi\sin\theta\cos\phi \\ \sin\psi\cos\theta & \cos\psi\cos\phi + \sin\psi\sin\theta\sin\phi & -\cos\psi\sin\phi + \sin\psi\sin\theta\cos\phi \\ -\sin\theta & \cos\theta\sin\phi & \cos\theta\cos\phi \end{bmatrix} \begin{bmatrix} a_x \\ a_y \\ a_z \end{bmatrix}
\end{aligned} \tag{20}$$

where a is the acceleration in the body frame measured by IMU, which is a combination of linear accelerations and the gravitational acceleration g; V is the velocity in the ECEM frame; θ, ϕ, and ψ are the aircraft pitch, roll, and heading angles, respectively. The aircraft kinematics nonlinear differential equations are then formulated into a 9-state continuous state-space model:

$$x = \begin{bmatrix} x \\ y \\ z \\ V_x \\ V_y \\ V_z \\ \phi \\ \theta \\ \psi \end{bmatrix}, \qquad u = \begin{bmatrix} a_x \\ a_y \\ a_z \\ p \\ q \\ r \end{bmatrix}, \qquad z = \begin{bmatrix} x \\ y \\ z \\ V_x \\ V_y \\ V_z \end{bmatrix} \tag{21}$$

$$\dot{x} = \begin{bmatrix} \dot{x} \\ \dot{y} \\ \dot{z} \\ \dot{V}_x \\ \dot{V}_y \\ \dot{V}_z \\ \dot{\phi} \\ \dot{\theta} \\ \dot{\psi} \end{bmatrix} = \begin{bmatrix} V_x \\ V_y \\ V_z \\ \cos\psi\cos\theta a_x + (-\sin\psi\cos\phi + \cos\psi\sin\theta\sin\phi)a_y + (\sin\psi\sin\phi + \cos\psi\sin\theta\cos\phi)a_z \\ \sin\psi\cos\theta a_x + (\cos\psi\cos\phi + \sin\psi\sin\theta\sin\phi)a_y + (-\cos\psi\sin\phi + \sin\psi\sin\theta\cos\phi)a_z \\ -\sin\theta a_x + \cos\theta\sin\phi a_y + \cos\theta\cos\phi a_z - g \\ p + q\sin\phi\tan\theta + r\cos\phi\tan\theta \\ q\cos\phi - r\sin\phi \\ (q\sin\phi + r\cos\phi)\sec\theta \end{bmatrix} + w \tag{22}$$

$$z = Hx + v = \begin{bmatrix} 1 & 0 & 0 & 0 & 0 & 0 & 0 & 0 & 0 \\ 0 & 1 & 0 & 0 & 0 & 0 & 0 & 0 & 0 \\ 0 & 0 & 1 & 0 & 0 & 0 & 0 & 0 & 0 \\ 0 & 0 & 0 & 1 & 0 & 0 & 0 & 0 & 0 \\ 0 & 0 & 0 & 0 & 1 & 0 & 0 & 0 & 0 \\ 0 & 0 & 0 & 0 & 0 & 1 & 0 & 0 & 0 \end{bmatrix} x + v \tag{23}$$

where x is the state vector to be estimated; u is the input vector, and z is the measurement vector, which is provide by the raw GPS measurement. This model is then discretized to be a set of nonlinear stochastic difference equations:

$$x_k = f(x_{k-1}, u_{k-1}, w_{k-1})$$

$$z_k = h(x_k, v_k)$$

$$\begin{bmatrix} x_k \\ y_k \\ z_k \\ V_{x_k} \\ V_{y_k} \\ V_{z_k} \\ \phi_k \\ \theta_k \\ \psi_k \end{bmatrix} = \begin{bmatrix} x_{k-1} + TsV_{x_{k-1}} \\ y_{k-1} + TsV_{y_{k-1}} \\ z_{k-1} + TsV_{z_{k-1}} \\ V_{x_{k-1}} + Ts(\cos\psi_{k-1}\cos\theta_{k-1}a_{x_{k-1}} + (-\sin\psi_{k-1}\cos\phi_{k-1} + \cos\psi_{k-1}\sin\theta_{k-1}\sin\phi_{k-1})a_{y_{k-1}} + (\sin\psi_{k-1}\sin\phi_{k-1} + \cos\psi_{k-1}\sin\theta_{k-1}\cos\phi_{k-1})a_{z_{k-1}}) \\ V_{y_{k-1}} + Ts(\sin\psi_{k-1}\cos\theta a_{x_{k-1}} + (\cos\psi_{k-1}\cos\phi_{k-1} + \sin\psi_{k-1}\sin\theta_{k-1}\sin\phi_{k-1})a_{y_{k-1}} + (-\cos\psi_{k-1}\sin\phi_{k-1} + \sin\psi_{k-1}\sin\theta_{k-1}\cos\phi_{k-1})a_{z_{k-1}}) \\ V_{z_{k-1}} + Ts(-\sin\theta_{k-1}a_{xk-1} + \cos\theta_{k-1}\sin\phi_{k-1}a_{y_{k-1}} + \cos\theta_{k-1}\cos\phi_{k-1}a_{zk-1} - g) \\ \phi_{k-1} + Ts(p_{k-1} + q_{k-1}\sin\phi_{k-1}\tan\theta_{k-1} + r_{k-1}\cos\phi_{k-1}\tan\theta_{k-1}) \\ \theta_{k-1} + Ts(q_{k-1}\cos\phi_{k-1} - r_{k-1}\sin\phi_{k-1}) \\ \psi_{k-1} + Ts(q_{k-1}\sin\phi_{k-1} + r_{k-1}\cos\phi_{k-1})\sec\theta_{k-1} \end{bmatrix} + w_{k-1} \tag{24}$$

$$z_k = Hx_k + v_k \tag{25}$$

where w and v are process and measurement noises, respectively. Both the process noise covariance matrix Q and measurement noise covariance matrix R are estimated based on the level of noise on previously acquired flight data using the same sensors:

$$Q = \begin{bmatrix} 0 & & & & & & & & & \\ & 0 & & & & & & & & \\ & & 0 & & & & & & & \\ & & & a_{x_{noise}} & & & & & & \\ & & & & a_{y_{noise}} & & & & & \\ & & & & & a_{z_{noise}} & & & & \\ & & & & & & p_{noise} & & & \\ & & & & & & & q_{noise} & & \\ & & & & & & & & r_{noise} & \end{bmatrix}$$

$$= \begin{bmatrix} 0 & & & & & & & & & \\ & 0 & & & & & & & & \\ & & 0 & & & & & & & \\ & & & 0.0014 & & & & & & \\ & & & & 0.0046 & & & & & \\ & & & & & 0.0091 & & & & \\ & & & & & & 1.8665e\text{-}004 & & & \\ & & & & & & & 6.0397e\text{-}004 & & \\ & & & & & & & & 1.5484e\text{-}004 & \end{bmatrix} \quad (26)$$

$$R = \begin{bmatrix} x_{noise} & & & & & \\ & y_{noise} & & & & \\ & & z_{noise} & & & \\ & & & V_{x_{noise}} & & \\ & & & & V_{y_{noise}} & \\ & & & & & V_{z_{noise}} \end{bmatrix}$$

$$= \begin{bmatrix} 0.0738 & & & & & \\ & 0.0036 & & & & \\ & & 0.0638 & & & \\ & & & 0.0017 & & \\ & & & & 0.0011 & \\ & & & & & 0.0078 \end{bmatrix} \quad (27)$$

For the EKF application, the nonlinear stochastic difference equations (5) and (6) are linearized at each time step. The Jacobian matrix of partial derivatives of f with respect to x is given by:

$$A_k = \begin{bmatrix}
1 & 0 & 0 & Ts & 0 & 0 & 0 & 0 & 0 \\
0 & 1 & 0 & 0 & Ts & 0 & 0 & 0 & 0 \\
0 & 0 & 1 & 0 & 0 & Ts & 0 & 0 & 0 \\
0 & 0 & 0 & 1 & 0 & 0 & \begin{matrix} Ts((\sin\hat{\psi}\sin\hat{\phi}+\cos\hat{\psi}\sin\hat{\theta}\cos\hat{\phi})a_y \\ +(\sin\hat{\psi}\cos\hat{\phi}-\cos\hat{\psi}\sin\hat{\theta}\sin\hat{\phi})a_z) \end{matrix} & \begin{matrix} Ts(-\cos\hat{\psi}\sin\hat{\theta}a_x+\cos\hat{\psi}\cos\hat{\theta}\sin\phi a_y \\ +\cos\hat{\psi}\cos\hat{\theta}\cos\hat{\phi}a_z) \end{matrix} & \begin{matrix} Ts(-\sin\hat{\psi}\cos\hat{\theta}a_x-(\cos\hat{\psi}\cos\hat{\phi}+\sin\hat{\psi}\sin\hat{\theta}\sin\hat{\phi})a_y \\ +(\cos\hat{\psi}\sin\hat{\phi}-\sin\hat{\psi}\sin\hat{\theta}\cos\hat{\phi})a_z) \end{matrix} \\
0 & 0 & 0 & 0 & 1 & 0 & \begin{matrix} Ts((-\cos\hat{\psi}\sin\hat{\phi}+\sin\hat{\psi}\sin\hat{\theta}\cos\hat{\phi})a_y \\ -(\cos\hat{\psi}\cos\hat{\phi}+\sin\hat{\psi}\sin\hat{\theta}\sin\hat{\phi})a_z) \end{matrix} & \begin{matrix} Ts(-\sin\hat{\psi}\sin\hat{\theta}a_x+\sin\hat{\psi}\cos\hat{\theta}\sin\hat{\phi}a_y \\ +\sin\hat{\psi}\cos\hat{\theta}\cos\hat{\phi}a_z) \end{matrix} & \begin{matrix} Ts(\cos\hat{\psi}\cos\hat{\theta}a_x+(-\sin\hat{\psi}\cos\hat{\phi}+\cos\hat{\psi}\sin\hat{\theta}\sin\hat{\phi})a_y \\ +(\sin\hat{\psi}\sin\hat{\phi}+\cos\hat{\psi}\sin\hat{\theta}\cos\hat{\phi})a_z) \end{matrix} \\
0 & 0 & 0 & 0 & 0 & 1 & \begin{matrix} Ts(\cos\hat{\theta}\cos\hat{\phi}a_y \\ -\cos\hat{\theta}\sin\hat{\phi}a_z) \end{matrix} & \begin{matrix} -Ts(\cos\hat{\theta}a_x+\sin\hat{\theta}\sin\hat{\phi}a_y \\ +\sin\hat{\theta}\cos\hat{\phi}a_z) \end{matrix} & 0 \\
0 & 0 & 0 & 0 & 0 & 0 & 1+T_s\tan\hat{\theta}_{k-1}(q_{k-1}\cos\hat{\phi}_{k-1}-r_{k-1}\sin\hat{\phi}_{k-1}) & T_s\sec^2\hat{\theta}_{k-1}(q_{k-1}\sin\hat{\phi}_{k-1}+r_{k-1}\cos\hat{\phi}_{k-1}) & 0 \\
0 & 0 & 0 & 0 & 0 & 0 & -T_s(q_{k-1}\sin\hat{\phi}_{k-1}+r_{k-1}\cos\hat{\phi}_{k-1}) & 1 & 0 \\
0 & 0 & 0 & 0 & 0 & 0 & T_s(q_{k-1}\cos\hat{\phi}_{k-1}-r_{k-1}\sin\hat{\phi}_{k-1}) & T_s\sec\hat{\theta}_{k-1}\tan\hat{\theta}_{k-1}(q_{k-1}\sin\hat{\phi}_{k-1}+r_{k-1}\cos\hat{\phi}_{k-1}) & 1
\end{bmatrix} \tag{28}$$

Jacobian matrix of partial derivatives of f with respect to w is given by:

$$W_k = I_{9\times 9} \tag{29}$$

Jacobian matrix of partial derivatives of h with respect to x is given by:

$$H_k = H \tag{30}$$

Jacobian matrix of partial derivatives of h with respect to v is given by:

$$V_k = H \tag{31}$$

Once the state-space model is formulated, the EKF follows the conventional time update equations:

$$\hat{x}_k^- = f(\hat{x}_{k-1}, u_{k-1}, 0) \tag{32}$$

$$P_k^- = A_k P_{k-1} A_k^T + Q_{k-1} \tag{33}$$

and measurement update equations:

$$K_k = P_k^- H_k^T (H_k P_k^- H_k^T + V_k R_k V_k^T)^{-1} \tag{34}$$

$$\hat{x}_k = \hat{x}_k^- + K_k(z_k - h(\hat{x}_k^-, 0)) \tag{35}$$

$$P_k = (I - K_k H_k) P_k^- \tag{36}$$

Figures 13-15 show the results from the EKF estimation, which is based on actual flight data acquired with one of the WVU YF-22 research aircraft. A high quality Goodrich Sensor Systems VG34® vertical gyro is also carried on-board to provide the reference attitude angle data for comparison purposes. Figures 13 and 14 demonstrate that the GPS/INS sensor fusion algorithm was able to provide a good estimation of aircraft attitude angle without the need for using expensive sensors.

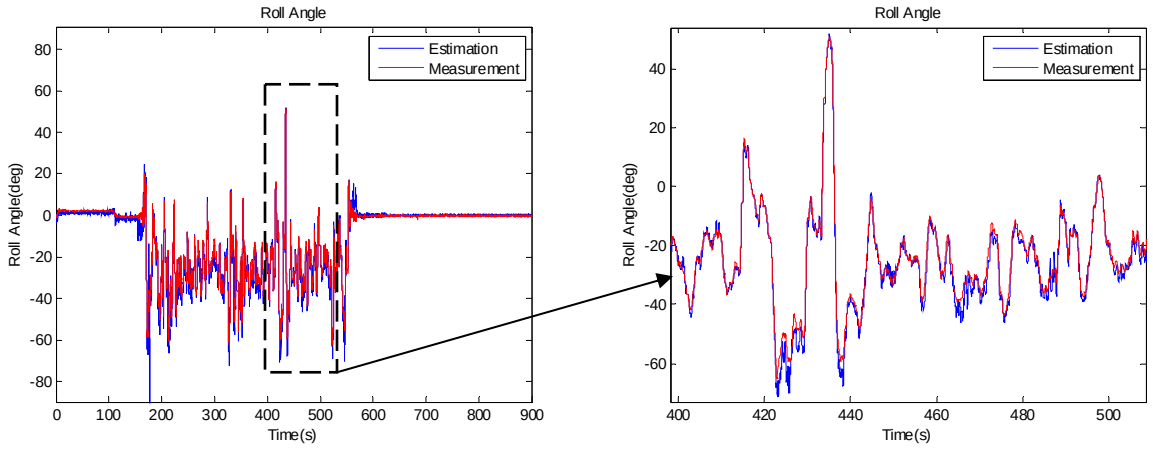

Fig. 13. EKF Roll Angle Estimation

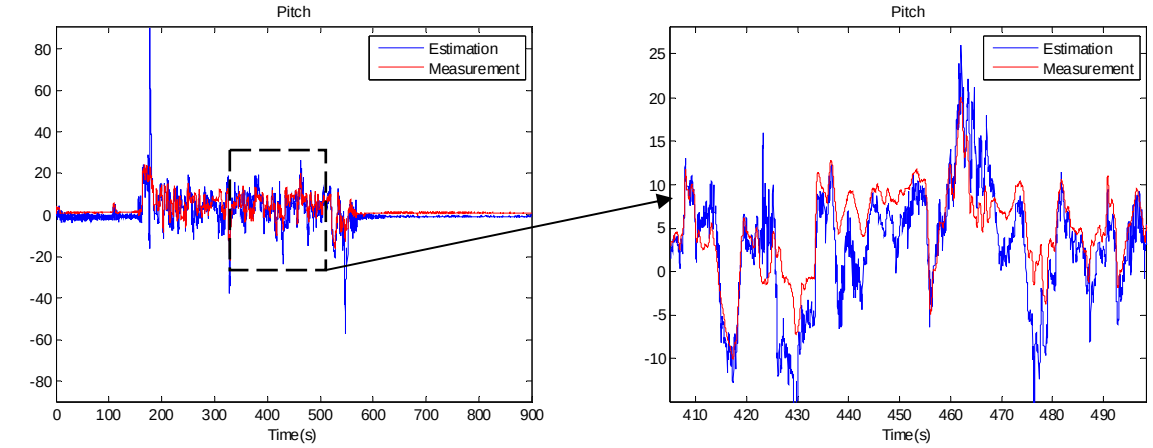

Fig. 14. EKF Pitch Angle Estimation

Figure 15 presents the GPS/INS position estimation when compared with the raw GPS measurements. Through the help of INS integration, the GPS/INS provides a very smooth position estimation that eliminated the large jumps typically seen in the raw GPS measurements.

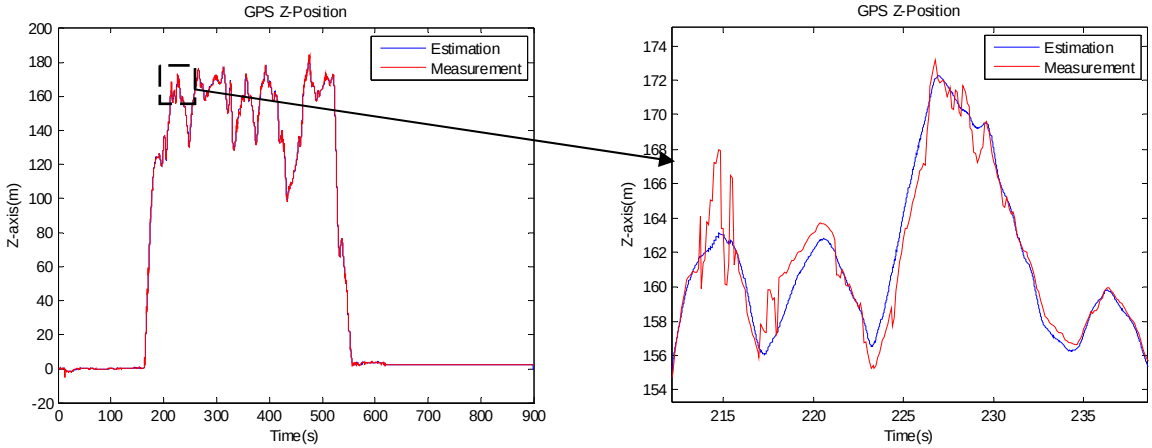

Fig. 15. EKF Position Estimation (Z-axis)

5. Conclusions

The successful completion of the project demonstrated that a low cost aerial platform could serve as a flexible tool for acquiring high-resolution geo-tagged images for ground areas of interest. The extraction of reliable information from these images could benefit DOT engineers in a variety of research areas including, but not limited to work zone management, traffic congestion, safety, and environmental. The development of the project also provided excellent opportunities for students to perform hands on research, and get educated in areas such as flight-testing, electronics, and software development.

Throughout this effort, valuable experience has been acquired on how to instrument and calibrate an aerial platform for imaging purpose, and how to plan and execute a flight-test session at remote locations. The post-flight image analysis has showed that it is possible to geo-reference ground assets based on a minimum Camera+GPS hardware configuration, although an improved position estimation performance can be achieved through a more delicate time-synchronization process and improved sensor measurements. A Time-Synchronization Board (TSB) and a GPS/INS sensor fusion algorithm have been developed for enabling these capabilities. The validation of these new capabilities will be performed in the near future.

References

[1] Harman, L.J., Shama, U., Dand, K., Kidwell, B., "Remote Sensing And Spatial Information For Transportation Demand Management (Tdm) Assessment", Proceedings of the Integrating Remote Sensing at the Global, Regional and Local Scale. Pecora 15/Land Satellite Information IV Conference, Denver, Colorado, 2002.

[2] "Use of Unmanned Air Vehicle (UAV) for Pipeline Surveillance to Improve Safety and Lower Cost", Project Report. Electricore, Inc. PHMSA Research and Development Contract Number: DTPH56-05-T-0004.

[3] HaLevi, E., "UAV's Deployed in Israel's Roads to Catch Violators", News Article, 09/15/05. Available: http://www.israelnationalnews.com/News/News.aspx/89924

[4] Haarbrink, R.B., Koers, E., "Helicopter UAV for photogrammetry and rapid response". Second International Workshop: The Future of Remote Sensing, Antwerp, October 2006.

[5] Zhang, C., "An UAV-based Photogrammetric Mapping System for Road Condition Assessment", Proceedings of Commission V, ISPRS Congress Beijing 2008.

[6] Farradyne, P.B. "Use of Unmanned Aerial Vehicles in Traffic Surveillance and Traffic Management - Technical Memorandum", May, 2005.

[7] Srinivasan, S., Latchman, H., Shea, J., Wong, T., and McNair, J. 2004. “Airborne Traffic Surveillance Systems: Video Surveillance of Highway Traffic,” In Proceedings of the ACM 2nd international Workshop on Video Surveillance &Amp; Sensor Networks (New York, NY, USA, October 15 - 15, 2004). VSSN '04. ACM, New York, NY, 131-135. DOI= http://doi.acm.org/10.1145/1026799.1026821

[8] Puri,A., "A Survey of Unmanned Aerial Vehicles for Traffic Surveillance", A Technical Report, University of South Florida, 2004.

[9] Gebre-Egziabher, D., "RPV/UAV Surveillance for Transportation Management and Security", Research Report No. CTS 08-27, December 2008.

[10] Coifman, B., McCord, M.R., Mishalani, R., Morris, S., Redmill, K., Ozguner, U., "Traffic Surveillance from an Uninhabited Aerial Vehicle", US DOT Workshop on Integration of PNT, RS, and Transportation The Ohio State Univeristy November 30, 2005.

[11] Heintz, F., Rudol, P., Doherty, P., "From Images to Traffic Behavior - A UAV Tracking and Monitoring Application". Proceedings of the Tenth International Conference on Information Fusion 2007, Québec, Canada, July, 2007.

[12] Puri, A. , Valavanis, K. P., Kontitsis, M., "Statistical Profile Generation for Traffic Monitoring Using Real-time UAV-based Traffic Video Data", Mediterranean Conference on Control and Automation - MED'07.

[13] Chen, Y. M., Dong, L., and Oh, J.-S., “Real-Time Video Relay for UAV Traffic Surveillance Systems Through Available Communication Networks”, in Proc. IEEE Wireless Communications and Networking Conference (WCNC), Mar. 2007.

[14] "Traffic Surveillance", Comet Projet (IST-2001-34304). Avaliable : http://www.comets-uavs.org/applications/traffic.shtml

[15] Rathinam, S., Almeida, P., Kim, Z., Jackson, S., Tinka, A., Grossman, W., Sengupta, R., "Autonomous Searching and Tracking of a River using an UAV", Proceedings of the 2007 American Control Conference, New York City, USA, July 2007.

[16] Brecher, A., Noronha, V., Herold, M., "A Roadmap For Deploying Unmanned Aerial Vehicles (UAVs) In Transportation - Summary Of Findings", Specialist Workshop, December 2, 2003, Santa Barbara, CA.

[17] FAA AFS-400 UAS POLICY 05-01 Unmanned Aircraft Systems Operations in the U. S. National Airspace System - Interim Operational Approval Guidance. September 16, 2005, Available: http://www.eoss.org/faa/AFS_400_UAS_POLICY_05_01.pdf

[18] FAA Interim Operational Approval Guidance 08-01, Unmanned Aircraft Systems Operations in the U. S. National Airspace System, March 13, 2008. Available:http://www.faa.gov/aircraft/air_cert/design_approvals/uas/reg/media/uas_guidance08-01.pdf

[19] FAA AC 91-57, Model Aircraft Operating Standards, June 09, 1981 Available:http://rgl.faa.gov/Regulatory_and_Guidance_Library/rgAdvisoryCircular.nsf/0/1acfc3f689769a56862569e70077c9cc/$FILE/ATTBJMAC/ac91-57.pdf

[20] K. Ro, J.-S. Oh, and L. Dong, "Lessons Learned: Application of Small UAV for Urban Highway Traffic Monitoring", in Proc. 45th AIAA Aerospace Sciences Meeting and Exhibit, Jan. 2007.

[21] FAA, Unmanned Aircraft Operations in the National Airspace System, 14 CFR Part 91, Docket No. FAA-2006-25714, February 6, 2007.

[22] National Geospatial – Intelligence, Length of a Degree of Latitude and Longitude, Available: http://www.nga.mil/MSISiteContent/StaticFiles/Calculators/degree.html

[23] Grewal, M. S., Weill, L.R., and Andrews, A.P., Global Positioning Systems, Inertial Navigation & Integration, 2nd ed., Wiley & Sons, New Jersey, Chap. 1, 2007.

[24] Ford, T., Neumann, J., Bobye, M., and Fenton, P., "OEM4 Inertial: A Tightly Integrated Decentralized Inertial/GPS Navigation System", Proceedings of ION GPS '01, Salt Lake City, Utah, Sept. 2001.